39th Plasmadynamics and Lasers Conference
23 - 26 June 2008, Seattle, Washington

AIAA 2008-4214

Aero-Optical Measurements in a Turbulent, Subsonic Boundary Layer at Different Elevation Angles

Jacob A. Cress*, Stanislav Gordeyev†
University of Notre Dame, Notre Dame, IN 46556

Martiqua L. Post‡
U.S. Air Force Academy, USAFA, CO 80840

and Eric J. Jumper§
University of Notre Dame, Notre Dame, IN 46556

This paper describes a recent investigation of aero-optical properties for subsonic turbulent boundary layers on a flat plate. Laser propagation through the boundary layer at several oblique elevation angles, Mach numbers, and boundary layer displacement thicknesses was investigated. A simple model is proposed that incorporates the oblique angle dependence into an existing scaling relationship. Both single and double boundary layers were investigated and the levels of optical distortions for propagation normal to the wall were found to be in good agreement with the refined scaling relationship. These new experimental data allowed us to both refine the scaling-relationship constant and reduce the error in the measurement below those presented in previous papers.

Nomenclature

f	=	frequency
f_{samp}	=	sampling frequency
I	=	instantaneous intensity on optical axis
I_0	=	diffraction limited, distortion-free intensity
K_{GD}	=	Gladstone-Dale constant
M	=	Mach number
OPD	=	optical path difference
OPD_{rms}	=	rms-of-OPD
OPL	=	optical path length
p'	=	pressure fluctuation
PSD	=	position-sensing device
q	=	dynamic pressure
St	=	Strouhal number
S_t	=	Strehl ratio
t	=	time
u	=	streamwise velocity component
u_τ	=	friction velocity
U_c	=	streamwise convection velocity
U_n	=	beam perpendicular convection velocity
U_∞	=	freestream velocity
x	=	streamwise coordinate
y	=	wall normal coordinate
β	=	elevation angle
δ	=	boundary layer thickness
δ^*	=	boundary layer displacement thickness
Δ	=	Malley probe beam spacing
θ	=	deflection angle or jitter
Λ	=	correlation length
λ	=	laser wavelength
ρ	=	freestream density
ρ_{SL}	=	sea level density
σ_ρ	=	mean-square density variance
σ_ϕ	=	mean-square phase error
τ	=	correlation time delay between beams
$+$	=	denotes wall unit

* Graduate Student, AME Department, B028 Hessert Laboratories, AIAA Student Member.
† Research Assistant Professor, AME Department, 122 Hessert Laboratories, AIAA Member.
‡ Assistant Professor, Department of Aeronautics, USAF Academy, CO, AIAA Member.
§ Professor, AME Department, 110 Hessert Laboratories, AIAA Fellow.

I. Introduction

AERO-OPTICS is concerned with the study of wavefront aberrations created by turbulent flow near an airborne laser exit pupil, typically within one or two aperture lengths. When a collimated laser beam, i.e. having a planar wavefront, passes through a turbulent flow field of variable-index-of-refraction, the laser-beam wavefront becomes aberrated. The performance of an optical system, be it free-space communication or directed-energy applications, can be severely degraded due to these aberrations.[1] Generally aero-optical aberrations are created by two types of flow: separated free-shear layers and turbulent boundary layers. The second of these two basic flows was investigated in the current study.

The optically-aberrating effects of high-speed, turbulent boundary layers have been the subject of research since the early 1950's. The first work in this area was by Liepmann[2] and was published as a Douglas Aircraft Company Technical Report. This report made use of the jitter angle of a thin beam of light as it traveled through the compressible boundary layer on the sides of high-speed wind tunnels as a way to quantify the crispness on Schlieren photographs. A significant piece of work was done in 1956 by Stine and Winovich[3]; they performed photometric measurements of the time-averaged radiation field at the focal plane of a receiving telescope in an attempt to validate Liepmann's formulation. Their work brought together all that had previously been done on optical propagation through index-variant turbulent flows. This work also raised the prospect of using an optical degradation measurement as a method of inferring turbulence scales. Based heavily on the approach taken by Tatarski[4] for electromagnetic waves propagated through the atmosphere, in the early 1960's Sutton[5] produced the most-widely referenced theoretical formulation for the aberrating effects of turbulent boundary layers based on statistical measures of the turbulence[2] and developed a "linking equation" between the turbulence quantities and the optical phase variance:

$$\sigma_\phi^2 = 2K_{GD}^2 k^2 \int_0^L \sigma_{\rho'}^2 \Lambda(y) dy \,. \qquad (1)$$

where σ_ϕ is the mean-square phase error, K_{GD} is the Gladstone-Dale constant, k is equal to $2\pi/\lambda$, σ_ρ is the mean-square density variance, and Λ is a correlation length.

Work on the turbulent boundary layer intensified in the late 1960's and through the decade of the 1970's due to an interest in placing lasers on aircraft. In the 1970's Rose[6] conducted the most extensive, at that time, experimental studies of optical aberrations caused by a turbulent boundary layer. Rose conducted hotwire measurements in turbulent boundary layers in order to obtain their density fluctuations, $\rho'(y)$, and associated correlation lengths, $\Lambda_\rho(y)$. These measurements were used to estimate wavefront aberrations that would be imprinted on a laser beam propagated through the same turbulent boundary layer assuming homogeneous turbulence. The on-average wavefront spatial aberrations, in the form of OPD_{rms}, were estimated using Sutton's linking equation, Eq. (1), but absent the k^2 term. Rose empirically found OPD_{rms} to be proportional to dynamic pressure, q, and boundary layer thickness, δ, such that $OPD_{rms} \sim q\,\delta$. It should be noted that in inferring $\rho'(y)$, Rose assumed that p' was negligible.

These aircraft hotwire measurements were complemented by the work of Gilbert[7], who performed interferometer measurements. In the Gilbert work, the interferometry used a double-pulse technique, which measured the difference in the wavefront from one pulse to another, rather than the distorted wavefront at a given instance, and only a limited number of these were made. Gilbert reported that the interferometry generally supported the hotwire integral-method estimations of the OPD_{rms}; however, based on his work, Gilbert concluded that the *square* of the OPD_{rms} is dependent linearly on the dynamic pressure, $OPD^2_{rms} \sim q$.

In 1994, Masson et al[8] revisited the Gilbert and Rose data and concluded that after removing systematic errors from Gilbert's data, $OPD_{rms} \sim (\rho\, M^2)^{1.16}$. He also found that there appeared to be a systematic difference between direct (i.e., interferometric) and indirect (i.e., the linking equation) wavefront error measurements, with the interferometric estimates consistently yielding higher estimates of the OPD_{rms} than the hotwire estimates, but he could not offer a reasonable explanation why optical and hotwire data did not agree.

The affect that aberrations have on the optical system can be measured with the time-averaged Strehl ratio, $\overline{S_t}$, which is defined as $\overline{S_t} = \dfrac{\bar{I}}{I_0}$, where I is the instantaneous intensity on the optical axis and I_0 is the diffraction limited, distortion-free intensity. The root-mean-squared optical path difference, OPD_{rms}, can be used to approximate the time-averaged Strehl ratio with the "large aperture approximation,"

$$\overline{S_t} = \exp\left[-\left(\frac{2\pi OPD_{rms}}{\lambda}\right)^2\right], \quad (2)$$

where λ is the laser wavelength.[9] Note that the exponent scales with the inverse of the wavelength squared. For a fixed OPD_{rms}, decreasing the lasing wavelength will have the effect of reducing the Strehl ratio. Lasers that were being used on airborne platforms in the 1960's and 1970's were CO_2 lasers that have a lasing wavelength of 10.6 μm. As a result, turbulent boundary layers were initially thought to have little or no impact on the optical system performance.[1] If the OPD_{rms} caused by a turbulent boundary layer were estimated to be 0.1 μm, the Strehl ratio would be approximately 0.996; however, reducing the laser wavelength to the near infrared (~1 μm), which is of particular interest today, has the effect of reducing the Strehl ratio to 0.674.

Based on the fact that newer lasers envisioned for airborne platforms have an order of magnitude shorter wavelength than those of the 1970's and 1980's, boundary-layer investigations picked up in mid-1990s, when the pioneering use of a Malley probe in making optical measurements in turbulent boundary layers[10] showed that the Malley probe gives the most accurate and highly time-resolved information about optical distortions with bandwidths exceeding 100 kHz. The Malley probe is described in the next section. Gordeyev et al[10], Wittich et al[11], and Buckner et al[12], have investigated the optical properties of the turbulent boundary layer using this technique. Gordeyev et al[10] made aero-optical measurements on a turbulent boundary layer at several Mach numbers and for various boundary layer thicknesses. From these tests, a scaling law was developed that related the OPD_{rms} to the density ratio at altitude, ρ, to sea level, ρ_{SL}, Mach number squared, M^2, and boundary layer displacement thickness, δ^*, $OPD_{rms} \sim \delta^* \frac{\rho}{\rho_{SL}} M^2$. Initially the scaling constant was found to be 2.4×10^{-5} (μm/mm). Wittich et al[11] refined the scaling constant value by improving the test section to reduce low-frequency vibration corruption of the Malley probe signal associated with the mirror being mounted in the test section. From their results, the scaling constant was refined from 2.4×10^{-5} to 1.6×10^{-5} (μm/mm) with an error of $\pm0.4\times10^{-5}$,

$$OPD_{rms} = 1.6\ (\pm 0.4) \times 10^{-5} \cdot \delta^* \frac{\rho}{\rho_{SL}} M^2. \quad (3)$$

Wittich's study also verified that an OPD_{rms} relationship exists when passing through a single turbulent boundary layer versus passing through two statistically independent turbulent boundary layers, so that,

$$OPD_{rms}^{Single\ TBL} = \frac{1}{\sqrt{2}} OPD_{rms}^{Double\ TBL}. \quad (4)$$

For the aero-optical studies of subsonic boundary layers mentioned above, measurements were taken only in the wall normal direction; to our knowledge no oblique propagation angles have ever been studied until the study described here. In one of the earlier studies by Buckner et al[12] of the aberrating character of high-Mach, subsonic turbulent boundary layers, the underlying aberrating structures were also investigated; it was found that there was a strong correlation between the convection of optically aberrating structures and unsteady pressure fluctuations in the outer portion of the boundary layer. It was further found that these aberrating, coherent structures convected past at approximately 0.8 of the freestream velocity. It has long been proposed that the coherent structures found in turbulent boundary layers have a "hairpin" shape. Many experiments have been performed on turbulent boundary layers to study these coherent structures; the reader is referred to Adrian et al[13] and Dargahi[14] for two in depth studies that measured the "hairpin" vortex packets with a variety of methods including flow visualization. Of particular interest to the current investigation, is the angularity of the vortex packets relative to the wall. Adrian et al[13] and Dargahi[14] both agreed that through some mechanism, the vortex packet is generated in the region near the wall and grows upwards as the vortex packet moves in the downstream direction. Depending on the particular region in the boundary layer the mean angle that the growing "hairpin" vortex makes with the wall varies from as small as 10° in the near wall region upwards to 45°-60° in the outer region. The angularity of the coherent "hairpin" vortex packets can be clearly seen in the flow visualization figures in each of the mentioned reports.

The goal of this study is to determine what effect the oblique elevation angle, β, of laser light propagation, has on the aero-optical environment in general, and specifically on the OPD_{rms} and the scaling laws developed by Gordeyev et al[3] and Wittich et al.[11]

II. Malley Probe

The Malley probe is an optical sensor based upon the technique introduced by Malley et al.[15] The operation of this instrument, which is described in detail in Ref. 16, assumes from Huygens' Principle that a small-aperture beam which passes through a variable-index-of-refraction field will emerge from that region perpendicular to the wavefront of a larger beam propagated through the same location at the same moment. Therefore, a time-record of the deflection of the small-aperture beam gives a history of the wavefront slope at that location. If the convection velocity, U_c, of the aberrating structures is known, the *OPD* can be found using,

$$\begin{aligned} OPL(t) &= -U_c \int_{t_0}^{t} \theta(t) dt \\ OPD(t) &= OPL(t) - \overline{OPL(t)} \end{aligned}, \qquad (5)$$

where *OPL* is the optical path length, t is time, θ is the deflection angle or jitter signal. A second-order quadrature integration scheme is used to compute the *OPD* from the jitter time series. Time is then traded for a pseudo-streamwise coordinate, x, using the frozen flow assumption, $x = -U_c\, t$, and wavefronts can be apertured for any given beam aperture.

A schematic of the Malley probe is shown in Figure 1. Two parallel laser beams are traversed through the turbulent flow with boundary layers on the tunnel walls and are reflected back along the same path using the return mirror. The jitter signal from each returning beam is measured with a position-sensing device, *PSD*. The current Malley probe uses duo-lateral sensors in each *PSD* in place of tetra-lateral sensors used in earlier studies. The duo-lateral *PSD* offers a linear response across the entire sensor face, which is an improvement over the non-linear edge effects of the tetra-lateral *PSD* (both duo- and tetra-lateral sensors were used in this current study). Instead of estimating the convection velocity, as done by Malley[15], the inclusion of the second beam allows the convection velocity to be directly calculated.[16] The jitter signals are correlated in the Fourier domain and the phase relation between the two beams, as a function of frequency, is determined. For a known separation between the two beams, the convection velocity as a function of frequency can be found from the slope of the phase/frequency plot, see Refs. [11, 16] for a detailed explanation of the phase/convection velocity relationship. The convective velocity is directly related to the beam's spacing; therefore accurate measurement of the beam's spacing is critical.

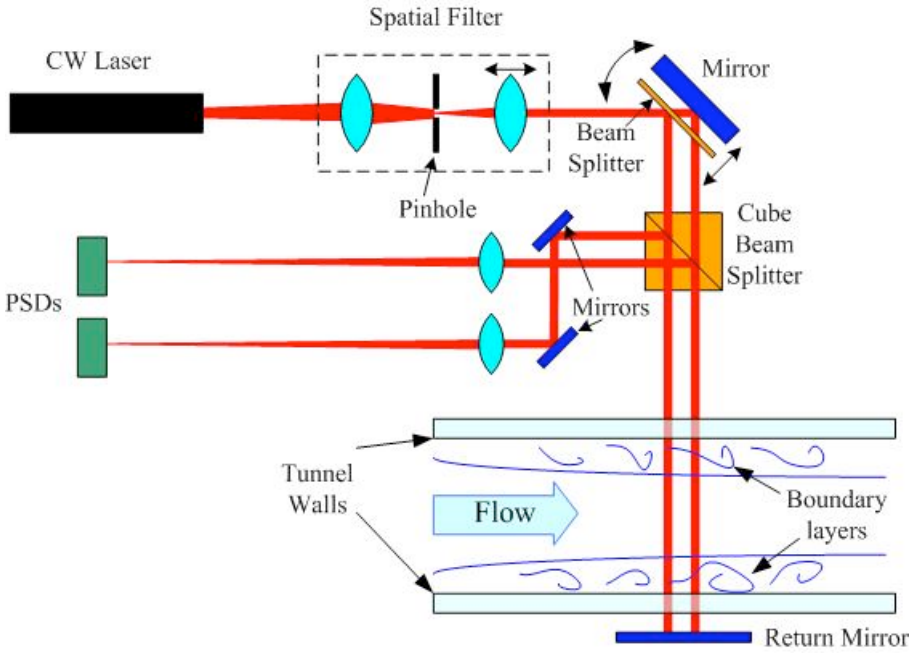

Figure 1: Schematic of the Malley probe as used with the turbulent boundary layer setup.

III. Experimental Setup

Turbulent boundary layer measurements were conducted in wind tunnel facilities at the University of Notre Dame and at the United States Air Force Academy, USAFA.

A. Notre Dame Experimental Setup

The first series of tests were performed in a transonic indraft wind tunnel located in the Hessert Laboratory at the University of Notre Dame. This tunnel is comprised of an inlet with a contraction ratio of 150:1, followed by a boundary-layer development section, measurement/test section, and diffuser, see Figure 2. The cross-section of the development and test sections measured 10.1 cm by 9.9 cm and are made of Plexiglas. Unlike the previous studies [10-12], the development section was not roughened, but the overall length from the beginning of the development section to the measurement section was increased to 170 cm to create a thicker boundary layer. The diffuser was connected to a large gated plenum. The pressure in the plenum was lowered using either one or two vacuum pumps to achieve the desired flow velocity in the test section. Air velocity was controlled by adjusting the rotation rate of the centrifugal pumps; fine adjustments to the plenum pressure were made with an exhaust valve.

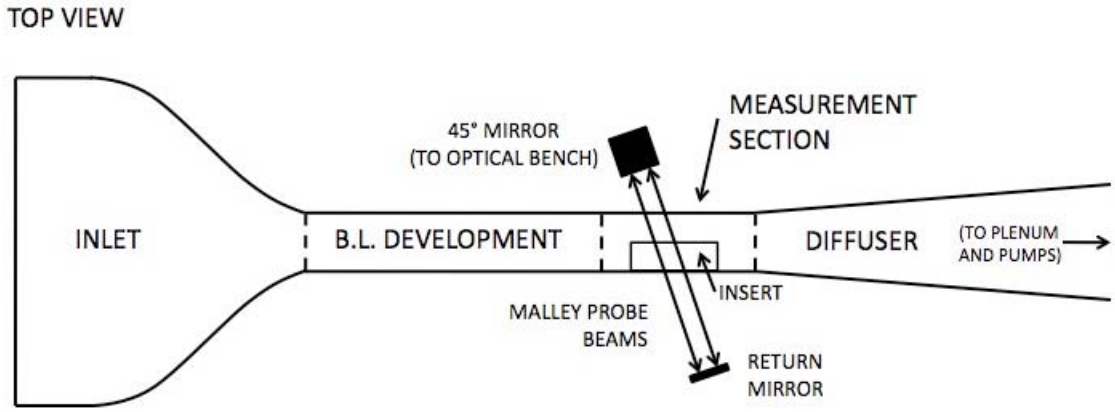

Figure 2: Schematic of the Notre Dame turbulent boundary layer test facility.

The Plexiglas boundary layer development sections were designed to allow hotwire access. A linear traverse mechanism could be placed in access ports at thirteen streamwise locations along the length of the development section. At each hotwire measurement location, total and static pressures were measured from which the local Mach number was computed. In the optical test section, total and static pressure ports were placed just upstream of the optical axis.

The purpose of this paper is to describe the impact the oblique angle had on the optical distortions due to a single boundary layer or due to passing through two (double) turbulent boundary layers, one on each side of the tunnel. Because low-frequency vibration hindered earlier investigations by both Gordeyev et al[10] and Wittich et al[11], a new method to study a single boundary layer was developed. Instead of placing the return mirror on a fixed platform inside of the test section, where it vibrated with the tunnel and significantly corrupted Malley probe data, a narrow optical insert, shown in Figure 3, was designed that protruded into the flow and effectively allowed the Malley probe laser beams to by-pass the boundary layer on one wall, see Figure 4a. The optical insert measured 100 mm in the streamwise direction, 5 mm in the spanwise direction and protruded 25 mm into

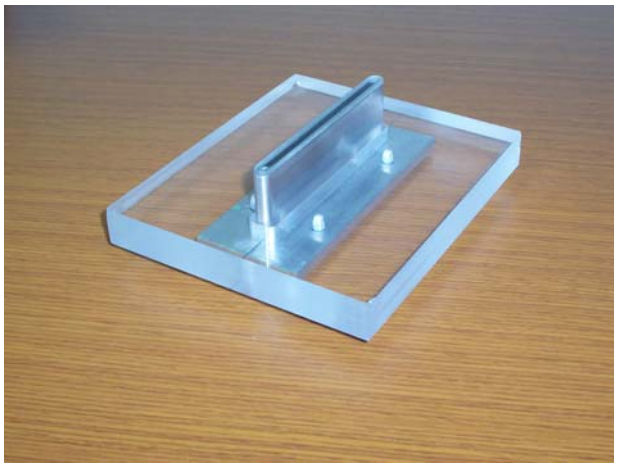

Figure 3: Optical insert for the Notre Dame tunnel.

the flow; the insert was capped with an optically transparent Plexiglas plate that was 3 mm thick. The internal length and height dimensions of the optical insert were sufficiently large to allow clearance of the Malley probe beams at oblique angles, β, ranging from 60° to 120°; note that the angle was defined as 0° facing the upstream direction and 180° in the downstream direction. Measurements were also made without the insert installed, so that the Malley probe beams passed through two boundary layers, one on each wall, see Figure 4b. Tested Mach numbers at the measurement section were 0.4, 0.5, and 0.6; and oblique angles tested were 60º, 70º, 80º, 90º and 110º.

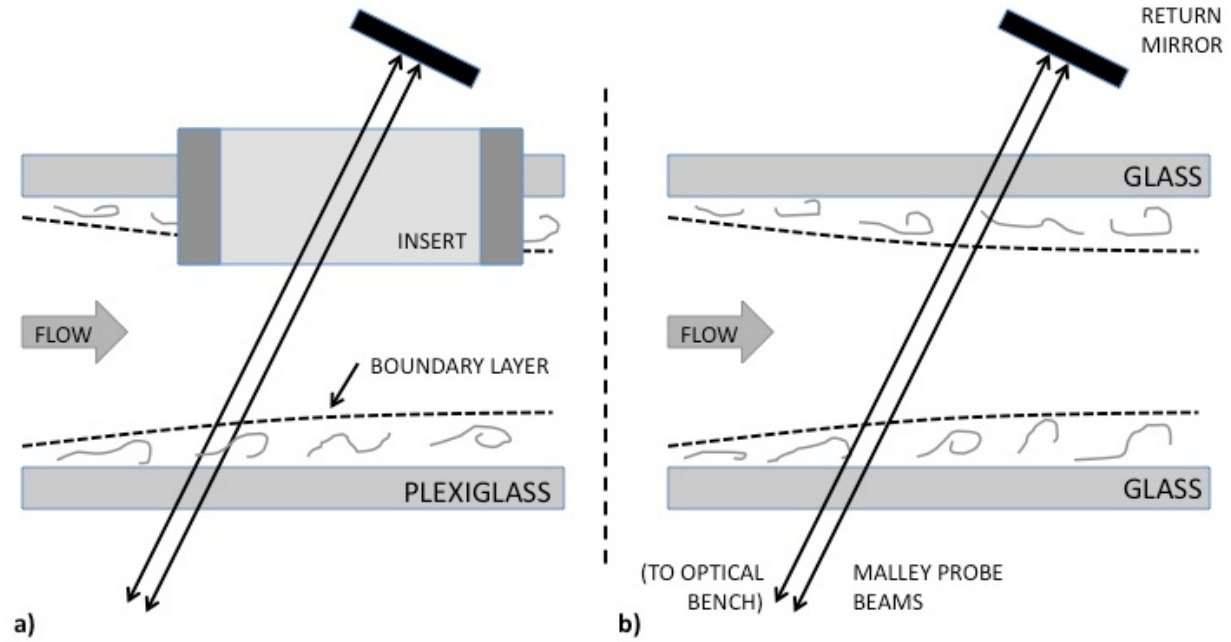

Figure 4: Schematics of the test section for a) single boundary layer measurements with the optical insert in place to by-pass the boundary layer on one wall and b) double boundary layer measurements.

B. USAFA Experimental Setup

The second set of tests was conducted in the Subsonic Wind Tunnel facility at the United States Air Force Academy in Colorado Springs, Colorado. This closed-loop tunnel has an 8 ft long test section with a cross-sectional area of 3 ft by 3 ft, see Figure 5a. The tunnel could achieve speeds in excess of Mach 0.5, but runtime at this high Mach number was limited due to tunnel motor heating. Both single and double boundary layer tests, as detailed in Figure 4, were performed in the USAFA wind tunnel for three incoming Mach numbers of 0.4, 0.45 and 0.5. For the thicker boundary layer at the USAFA, a larger optical insert was built, see Figure 5b. The length of the new insert in the streamwise direction was 250 mm, 10 mm in the spanwise direction, and it protruded 40 mm into the test section. The Plexiglas viewing port was 5 mm thick. For the single boundary layer tests with the optical insert, the tested elevation angles were 48º, 90º, 124º and 133º; these angles being constrained by optical access to the tunnel. For the double boundary layer tests, elevation angles were 90º, 116º, 126º, 132º and 140º.

IV. Results

A. Hotwire Results

Velocity profiles were taken in the Notre Dame wind tunnel facility using a single boundary layer hotwire probe at a freestream velocity of Mach 0.5. Thirteen streamwise locations along the length of the development and test sections were measured. A TSI, Inc, IFA-100 Intelligent Flow Analyzer was used to acquire, condition and high-pass filter the hotwire data. The normalized mean, $U(y)$, and root mean squared, $U_{rms}(y)$, velocity profiles at each x location are shown in Figure 6a, where the velocity is normalized by the freestream velocity, U_∞, and the wall normal coordinate, y, is normalized by the displacement thickness, δ^*. At the optical measurement location, approximately 170 cm downstream of the inlet, the displacement thickness was found to be approximately 3.3 mm at Mach 0.5, and the friction velocity, u_τ, was found to be approximate 5.5 m/s using Clauser's Method. Figure 6b shows the velocity profile in wall units, y^+. The velocity profile is plotted against the log-law relationship,

$$u^+ = \frac{1}{\kappa}\log y^+ + B, \qquad (6)$$

where κ was 0.41 and B was 5.6. The small increase of the velocity in the near wall, occurring below 100 wall units, or 0.2 mm in physical units, is likely due to a hotwire/wall interaction.

For USAFA tests, boundary layer velocity data were collected by the USAFA.[17] From the provided data, the displacement thickness was calculated at each of the optical measurement stations for the three Mach numbers studied, with values ranging from 2.0 mm near the inlet to upwards of 3.5 mm at the most downstream window.

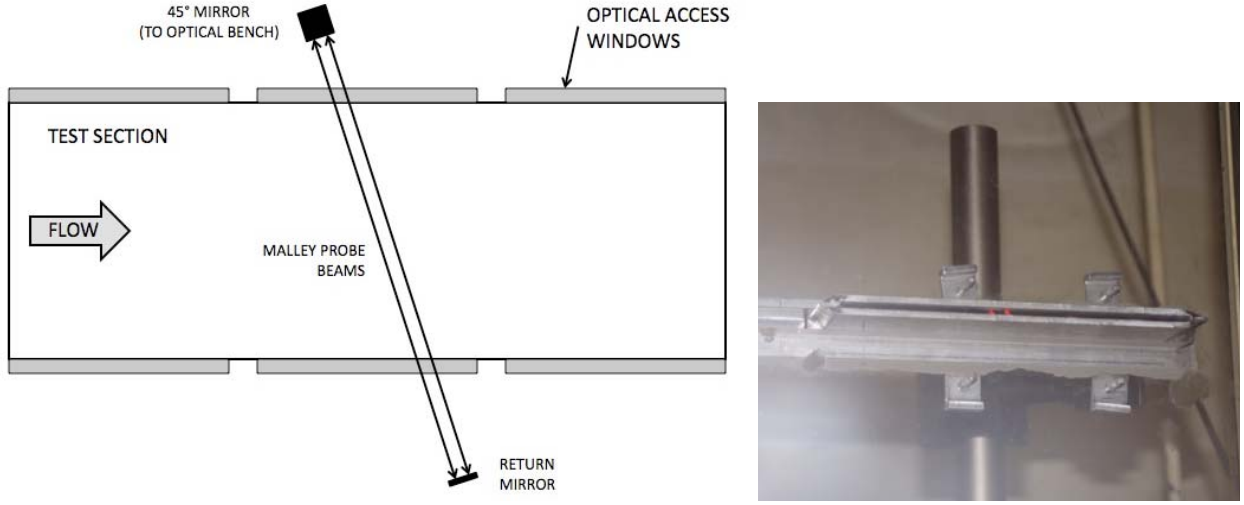

a) b)

Figure 5: a) Schematic of the USAFA wind tunnel facility. b) Optical insert for USAFA tunnel.

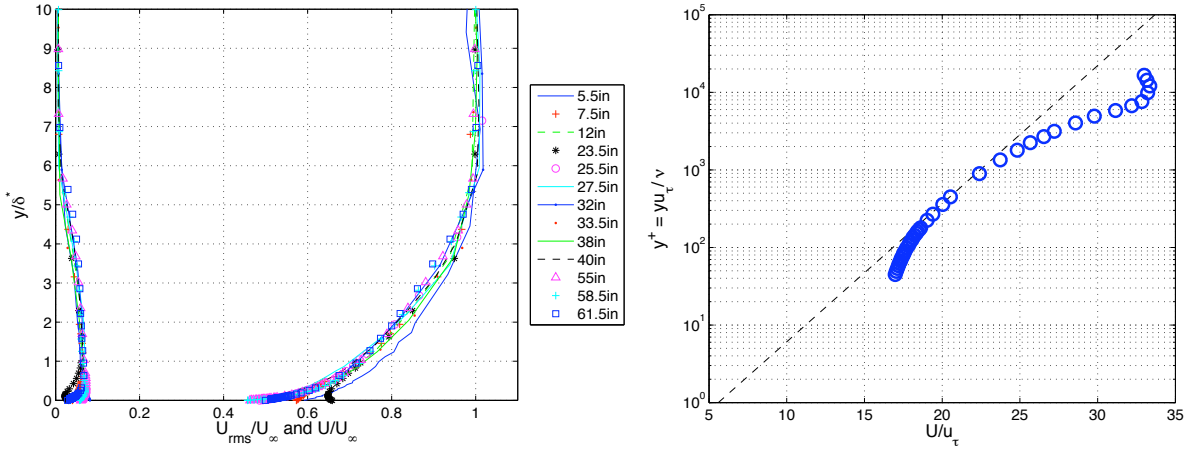

a) b)

Figure 6: a) Normalized hotwire velocity profiles (mean and rms) of the upper wall boundary layer of Notre Dame transonic wind tunnel at 13 streamwise locations. b) Boundary layer profile in wall units at the optical test section. The friction velocity is 5.5 m/s. The dashed line represents the log-law, Eq. (6).

B. Malley Probe Results

1. *Deflection Angle Spectral Analysis*

In Ref. 11 it was shown at the elevation angle of 90º, for OPD_{rms} to follow the "ρM^2" law, Eq. (3), the deflection angle spectrum $\hat{\theta}(f)$ should scale as,

$$\hat{\theta}(f) = \frac{\rho}{\rho_{SL}} M^2 \frac{\delta^* f_{samp}}{U_\infty} \hat{\theta}_{norm}\left(\frac{f\delta^*}{U_\infty}\right). \quad (7)$$

It had been suggested that for non-normal propagation at an oblique angle, β, since the beam would traverse a longer distance of $\delta^*/\sin(\beta)$ through the boundary layer, the scaling law may only need to be corrected by this additional distance. That is, to simply account for oblique angle effects on OPD_{rms}, replace δ^* with $\delta^*/\sin(\beta)$ in Eq. (3);

$$OPD_{rms} \sim \frac{\delta^*}{\sin(\beta)} \frac{\rho}{\rho_{SL}} M^2. \quad (8)$$

However, deriving a correct scaling for deflection angle spectra for oblique propagation requires an understanding of the original scaling derivation. As described in Refs. [11, 16], the wavefront, *OPD*, was calculated from the deflection angle, $\theta(t)$, assuming a frozen convective speed. But, as the diagram in Figure 7 shows, the convective speed *in the direction normal to the laser beams* is $U_n = \Delta/\tau$, where τ the correlation time delay between the upstream and downstream beam. The Malley probe measures U_n, which must not be confused with the *total* convective speed, U_c, where $U_c = \Delta/[\tau \sin(\beta)] = U_n/\sin(\beta)$. Therefore, Eq. (5), for an arbitrary oblique angle should be written as,

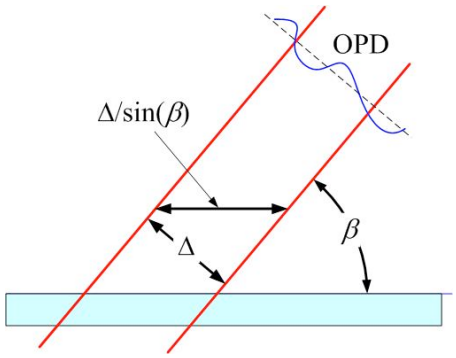

Figure 7: Malley probe calculation of *OPD* for an oblique elevation angle.

$$OPD \sim U_n \int \theta(t)dt = U_c \sin(\beta) \int \theta(t)dt. \quad (9)$$

Combining Eqs. (8) and (9) gives the proper scaling for the deflection angle spectrum with elevation angle dependence as,

$$\hat{\theta}(f) = \frac{\rho}{\rho_{SL}} M^2 \frac{\delta^* f_{samp}}{U_\infty} \frac{1}{\sin^2(\beta)} \hat{\theta}_{norm}\left(\frac{St}{\sin(\beta)}\right), \quad (10)$$

where $St = f\delta^*/U_\infty$ is the Strouhal number.

Total convective speeds measured directly by the Malley probe were found to be approximately 0.83 of the freestream speed for all Mach numbers and elevation angles tested. These values are close to convective speeds values of 0.87 of the freestream speed reported in [11].

Examples of un-scaled double boundary layer deflection angle spectra taken at the USAFA for three Mach numbers at the oblique angle of 116º are presented Figure 8. The large increase in spectra amplitude at low frequencies, below 500 Hz, are due to mechanical vibrations of the tunnel and the

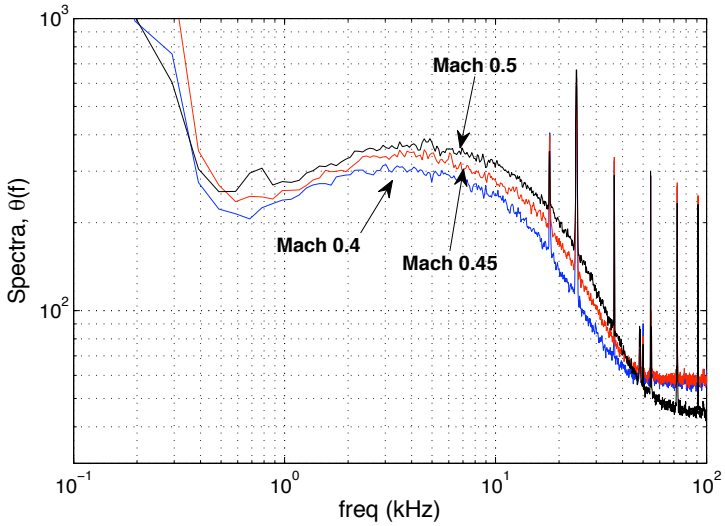

Figure 8: Un-scaled USAFA deflection angle spectra for three Mach numbers at one elevation angle of 116º.

return mirror, as well as to slow drift of the mean speed of the tunnel. This part of the spectrum was filtered prior to wavefront reconstruction using a high-pass filter with a cut-off frequency at 500 Hz. A broad hump in spectra centered around 5-7 kHz is due to the optical distortion of the boundary layer. The series of sharp peaks at the high-end of the frequency range are electronic noise.

When spectral results were scaled only with Mach number, using Eq. (7), they collapse for each oblique angle, see Figure 9a, further validating the "ρM^2" scaling found in earlier studies, see Refs. [10, 11]. For the double boundary layer tests, the equivalent displacement thickness was calculated by averaging the thicknesses of the two boundary layers at each streamwise location where the Malley probe laser beams traversed on either side of the tunnel. The scaled results, using the oblique-angle dependence in Eq. (10), are shown in Figure 9b. Scaled spectra show some collapse toward a "single" curve with a peak around $St/\sin(\beta) = 0.09$; however, the imperfect collapse suggests there are more things occurring.

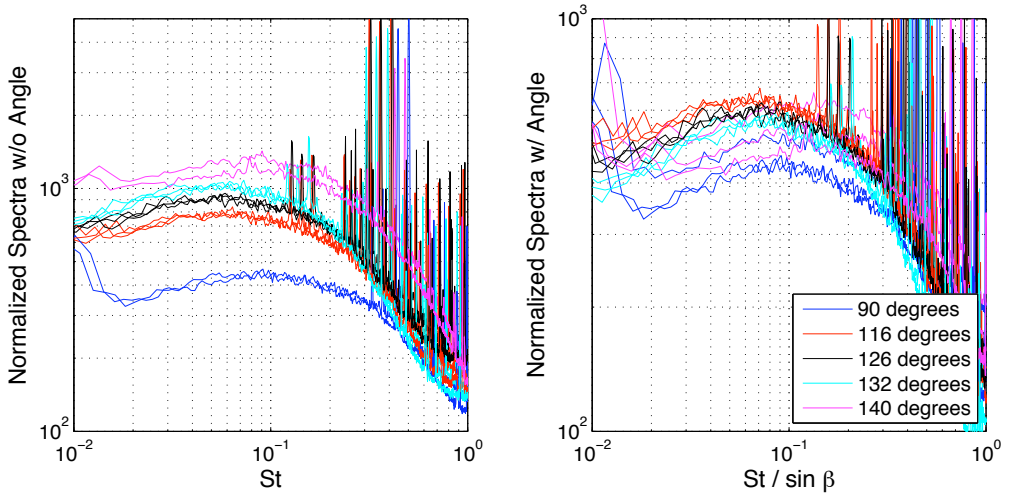

Figure 9: USAFA double boundary layer for three Mach numbers (denoted by same color) and five elevation angles. a) Spectra data normalized using Eq. (7). b) Normalized spectra data, with the inclusion of elevation angle dependence Eq. (10), as a function of $St/\sin\beta$.

To investigate the reasons for this imperfect collapse, deflection angle spectra from the *single* boundary layer measurements were scaled using the angular dependence, Eq. (10); the results are shown in Figure 10. As with the double boundary layer, the single boundary layer data collapsed nicely for all Mach numbers (not shown), yet there are still noticeable disparities between different elevation angles. For instance, focusing on scaled results for the upstream angle of 48º and its symmetric angle from the vertical, an oblique angle of 133º, the simple angular dependence scaling argument of Eq. (10) does not yield the identical spectra that we would expect, since $\sin(48º) \approx \sin(133º)$. Instead, as Figure 10 shows, the 133º case is consistently higher than the 48º case in the range of normalized frequencies $St/\sin(\beta)$ from 0.06 to 0.5. As was mentioned in the Introduction, the turbulent boundary layer has packets of vortical structures with a preferred angular direction, see Figure 11, thus exhibiting an *anisotropic* behavior. As a consequence, one would expect that when the laser beam goes in the downstream direction, it travels along these

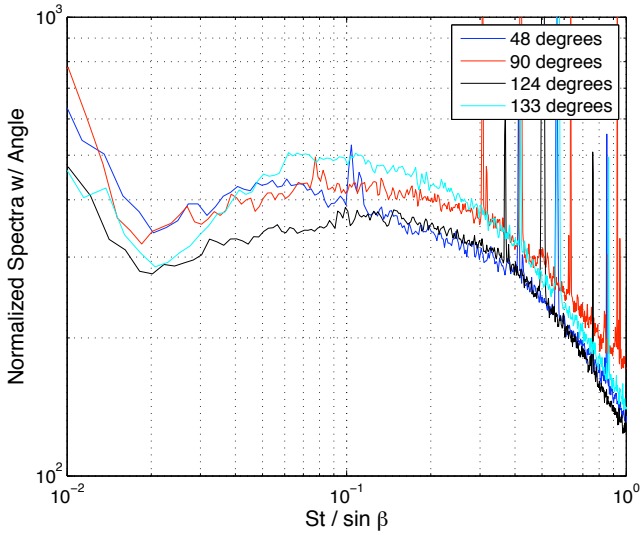

Figure 10: USAFA single boundary layer normalized spectra with angular dependence as a function of $St/\sin\beta$ for Mach 0.5 and 4 elevation angles.

elongated structures and becomes more aberrated, than when it travels in the symmetrical upstream direction. Indeed, this is what we observe in the normalized oblique-angle spectra. As seen in Figure 10, this holds true except for the 124º case, where the deflection angle spectrum drops below all other spectra. The reason for this anomaly is unclear and will require additional investigation.

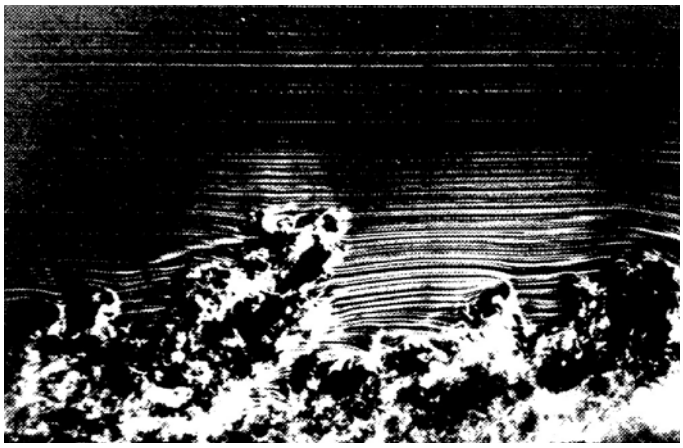

Figure 11: Elongated vortical structures in the turbulent boundary layer, flow goes from left to right. [Ref. 18]

Scaled results of single boundary layer measurements taken at Notre Dame are shown in Figure 12a; narrow peaks around St/sin(β) = 0.04 are due to tunnel-induced vibrations. For a fixed oblique angle, results collapse across Mach numbers tested (not shown in Figure 12a for clarity), but scaled data also exhibit anisotropic behavior with the 110º case being higher than for cases with lower oblique angles; these results are similar to the USAFA single boundary layer data.

Deflection spectra at 90º for the USAFA and Notre Dame tests are compared in Figure 12b. Deflection angle spectra collapse onto a single curve, verifying that the boundary layers are similar in both facilities, further validating the universality of the scaling law. The location of the boundary-layer-related hump is about St = 0.1 for both Notre Dame's single boundary layer and the USAFA's single and double boundary layer data. The location of the boundary layer hump is also in agreement with the earlier findings of Wittich.[11]

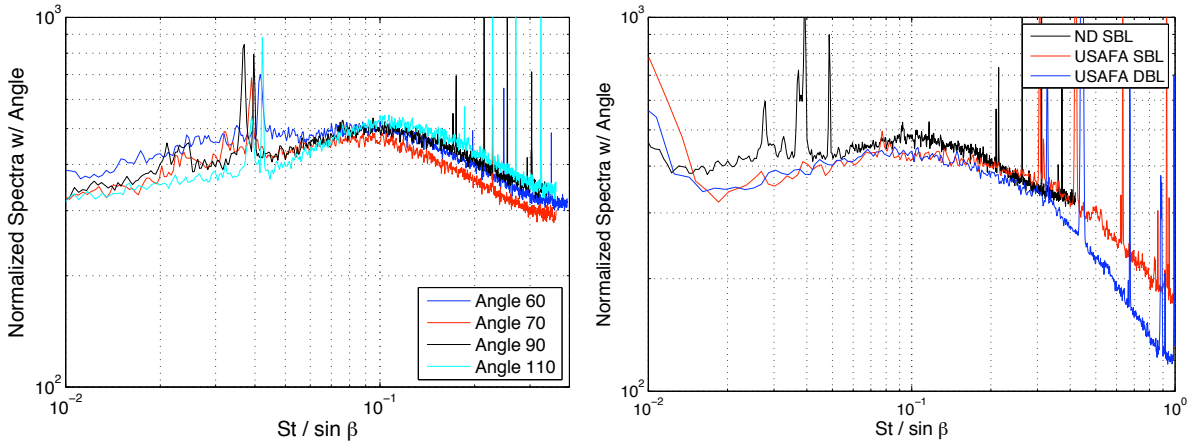

a) **b)**

Figure 12: a) Notre Dame single boundary layer normalized jitter spectra with angular dependence as a function of *St*/sin β for M = 0.6 and 4 elevation angles. b) 90º cases at M = 0.5 for the single boundary layer at Notre Dame and the USAFA and for the double boundary layer at the USAFA.

2. OPD_{rms} Results.

From the deflection angle temporal data, one-dimensional wavefront slices were constructed.[16] The wavefront results were apertured to 0.25 m and the average of rms-of-wavefront over the aperture, or OPD_{rms}, were calculated for all cases.

The wavefront results for the USAFA double boundary layer tests are plotted in Figure 13 versus the angular dependence, i.e., Eq. (8). Since in these tests the laser beam traversed through two boundary layers, the levels of optical aberrations for a single boundary layer were estimated from OPD_{rms} for double boundary layers using Eq. (4). The results collapse reasonably well onto a single line for all Mach numbers and oblique angles. The least-square analysis gives the best linear fit (shown as a dotted line) with a constant slope of 1.83 x 10^{-5}. This value is close to the value of 1.6 x 10^{-5}, reported by Wittich.[11]

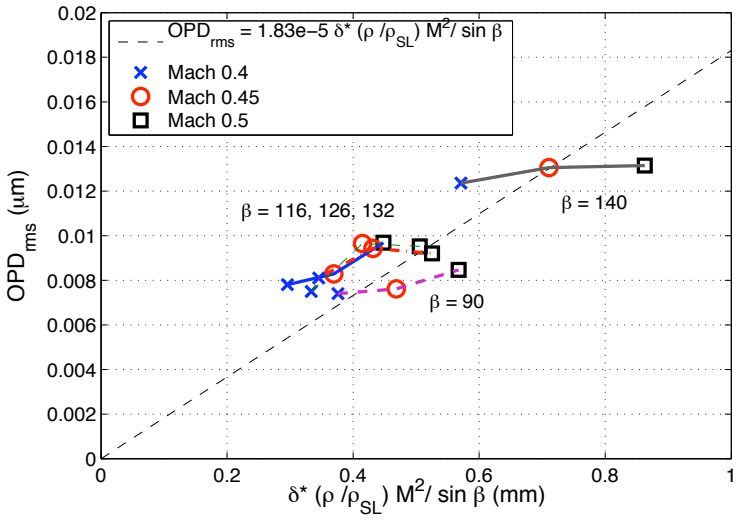

Figure 13: USAFA double boundary Layer OPD_{rms} scaling. Three Mach numbers and five elevation angles are shown.

Wavefront results for the USAFA single boundary layer tests are shown in Figure 14. The 48º and 90º cases collapse onto a single line. However, the look-back elevation angles are slightly higher than the forward-looking angles; these results are consistent with the anisotropic behavior of the boundary layer, discussed earlier. An overall slope, marked by a dashed line in Figure 14, was found to be approximately 1.6 x 10^{-5}.

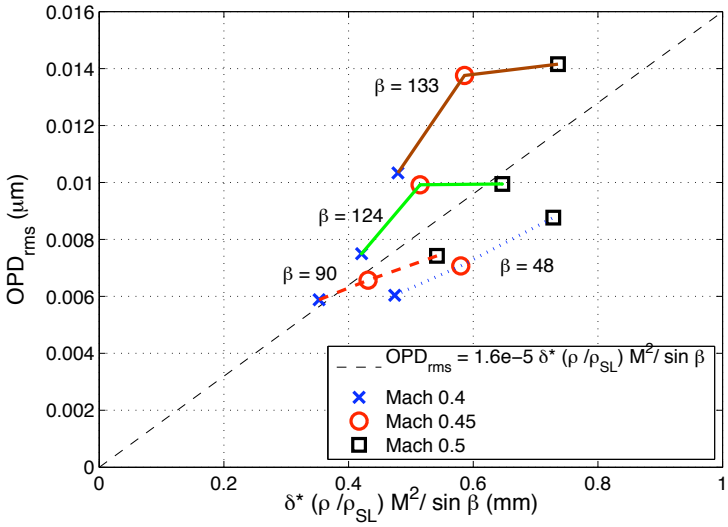

Figure 14: USAFA single boundary Layer OPD_{rms} scaling. Three Mach numbers and four elevation angles are shown.

Wavefront results for the Notre Dame single boundary layer are plotted in Figure 15. They also collapse to a single line; the slope was found to be 1.65 x 10^{-5}, which is right between the values of linear fits from the USAFA single and double boundary layer tests. Additionally, all of these scaling constants are within the range of uncertainty of the linear fit, 1.6 (± 0.4) x 10^{-5}, reported in the previous paper.[11] Results also reveal anisotropy of the boundary layer, with values for back-looking angles being consistently higher that for forward-looking angle cases.

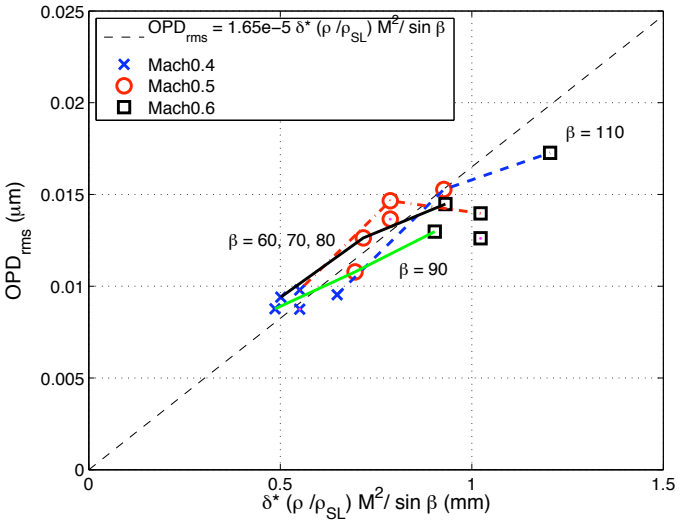

Figure 15: Notre Dame single boundary Layer *OPD$_{rms}$* scaling. Three Mach numbers and five elevation angles are shown.

Combining results from the USAFA and Notre Dame tests of optical distortions caused by turbulent boundary layers, an improved scaling including oblique propagation angle effects can be written as,

$$OPD_{rms} = 1.7\ (\pm 0.2)\cdot 10^{-5}\ \frac{\delta^*}{\sin(\beta)}\ \frac{\rho}{\rho_{SL}}\ M^2 . \qquad (11)$$

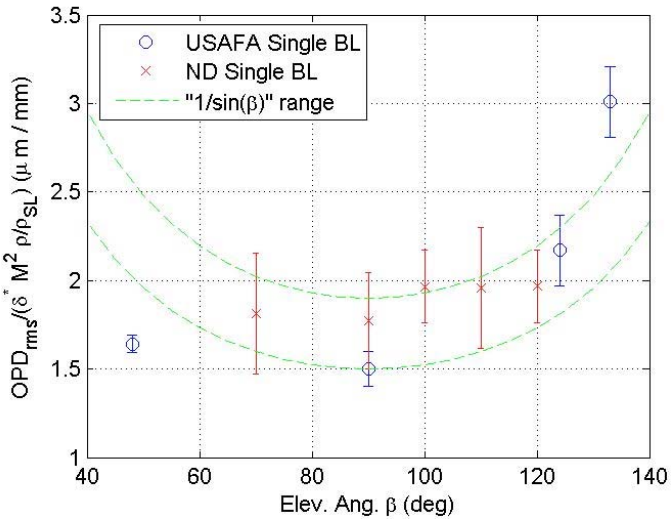

Figure 16: Single boundary layer *OPD$_{rms}$* data versus the elevation angle.

Note that this simple empirical relation does not include anisotropic behavior of optically-aberrating structures in the turbulent boundary layer. To see this more clearly, both the USAFA and Notre Dame *OPD$_{rms}$* results, normalized only by $\delta^*(\rho/\rho_{SL})\,M^2$, are plotted versus the oblique angle in Figure 16. Also, the "isotropic" oblique-angle dependence, "1/sin(β)" from Eq. (11), is plotted in Figure 16. While the "isotropic" curve-fit does a reasonable job

for oblique angles between 70º and 120º, it overestimates optical aberrations at forward-looking angles below 50º and underestimates optical distortion above 130º.

V. Conclusions

This paper has presented additional results for optical propagation normal to the wall through an optically-aberrating turbulent boundary layer. Further, results for propagation at oblique angles through the boundary layer have been presented. These data were collected in two separate tunnels with very different tunnel operating and flow-conditioning characteristics, yet the results show nearly the same trends and amplitudes. For laser beams propagated normal to the tunnel walls, the results are in good agreement with the results of previous studies, further validating the universality of the scaling laws given here and in previous papers and further refining and reducing the uncertainty of the law's constant. With the addition of the oblique angle propagation data, a simple scaling law has been proposed to roughly estimate the effect of elevation angle. Overall, the proposed simple model, Eq. (11), was found to satisfactory predict the average OPD_{rms} for different oblique angles. This simple empirical expression can be used to predict boundary-layer-related effects on an average far-field intensity on target for a given laser wavelength using Eq. (2).

On the other hand, the simple model does not account for the difference in propagation symmetrically up and downstream from normal. This anisotropy of oblique propagation appears to be consistent with what one might expect from descriptions found in other papers dealing with the vertical inclinations found on coherent vertical structures in turbulent boundary layers. This consistency with the findings of others regarding the structure of turbulence in a turbulent boundary layer also gives avenues of study associated with determining the physical cause of the aberrating character of the turbulent boundary layer that will be the subject of future papers. In the very least, this study has uncovered yet another aspect of predicting the aero-optical environment posed by a turbulent boundary layer and has once again pointed toward the prospects of studying the structure of turbulent boundary layers by examining its effect on the propagation of lasers through it, first alluded to by Stein and Winovich.[3]

Acknowledgments

The authors are grateful to the United States Air Force Academy Subsonic Tunnel personnel for technical assistance during tests; especially Ken Ostasiewski and cadets Andrew Roberts and David Butzin for their assistance in data collection. This effort was sponsored in part by the Office of Naval Research, under contract N00014-07-1-0291. The U.S. Government is authorized to reproduce and distribute reprints for government purposed notwithstanding any copyright notation thereon.

References

[1]Jumper, E. J., and Fitzgerald, E. J., "Recent advances in aero-optics," *Progress in Aerospace Sciences*, Vol. 37, 2001, pp. 299-339.

[2]Liepmann, H. W., "Deflection and diffusion of a light ray passing through a boundary layer," Report SM-14397, Douglas Aircraft Company, Santa Monica Division, Santa Monica, California, May 1952.

[3]Stine, H. A., Winovich, W., "Light diffusion through high-speed turbulent boundary layers," Research Memorandum A56B21, NACA, Washington, May 1956.

[4]Tatarski, V. I., *Wave Propagation in Turbulent Medium*, Dover, New York, 1961.

[5]Sutton, G. W., "Effects of turbulent fluctuations in an optically active fluid medium," *AIAA Journal*, Vol. 7, No. 9, 1969, pp. 1737–1743.

[6]Rose, W. C., "Measurements of Aerodynamic Parameters Affecting Optical Performance," Air Force Weapons Laboratory Final Report, AFWL-TR-78-191, May 1979.

[7]Gilbert, K. G., "KC-135 Aero-Optical Boundary-Layer/Shear-Layer Experiments," *Aero-Optical Phenomena*, Eds. K.G. Gilbert and L.J. Otten, Vol. 80, *Progress in Astronautics and Aeronautics*, AIAA, New York, 1982, pp. 306-324.

[8]Masson, B., Wissler, J., and McMackin, L., "Aero-Optical Study of a NC-135 Fuselage Boundary Layer," AIAA 1994-0277, January 1994.

[9]Smith, W. J., *Modern Optical Engineering: The Design of Optical Systems*, McGraw-Hill, NY, 1966, Chapter 3, pp. 49-71.

[10]Gordeyev, S., Jumper, E. J., Ng, T. T., and Cain, A. B., "Aero-Optical Characteristics of Compressible, Subsonic Turbulent Boundary Layers," *34th AIAA Plasmadynamics and Lasers Conference*, AIAA-2003-3606, Orlando, FL, 23-26 June 2003.

[11]Wittich, D. J., Gordeyev, S., and Jumper, E. J., "Revised Scaling of Optical Distortions Caused by Compressible, Subsonic Turbulent Boundary Layers," *38th AIAA Plasmadynamics and Lasers Conference*, AIAA-2007-4009, Miami, FL, 25-28 June 2007.

[12]Buckner, A., Gordeyev, S., and Jumper, E. J., "Optical Aberrations Caused by Transonic Attached Boundary Layers: Underlying Flow Structure," *43rd AIAA Aerospace Sciences Meeting and Exhibit*, AIAA-2005-0752, Reno, NV, 10-13 January 2005.

[13]Adrain, R. J., Meinhart, C. D., and Tomkins, C. D., "Vortex organization in the outer region of the turbulent boundary layer," *Journal of Fluid Mechanics*, Vol. 422, 2000, pp. 1-54.
[14]Dargahi, B., "Generation of Coherent Structures in Turbulent Boundary Layers," *Journal of Engineering Mechanics*, July 1997, pp. 686-695.
[15]Malley, M., Sutton, G. W., and Kincheloe, N., "Beam-Jitter Measurements for Turbulent Aero-Optical Path Differences", *Applied Optics*, Vol. 31, 1992, pp. 4440-4443.
[16]Gordeyev, S., Hayden, T., and Jumper, E. J., "Aero-Optical and Flow Measurements Over a Flat-Windowed Turret," *AIAA Journal*, Vol. 45, No. 2, 2007, pp. 347-357.
[17]Dumas, J., Fuqua, M., and Hayden, T., "Final Report: Boundary Layer Survey of the Subsonic Wind Tunnel," Department of Aeronautics, United States Air Force Academy, May 2005.
[18]Van Dyke, M., *An Album of Fluid Motion*, The Parabolic Press, Stanford, CA, 1982, p. 92.